

# Characterization, Compressive Strength and Output Voltage Properties of Silica/Barium Titanate Nanocomposite for Piezoelectric Applications

Muhammad Sadat Hamzah\* and Muhammad Syaiful Fadly

Department of Mechanical Engineering, Universitas Tadulako, Palu, Indonesia

Muhammad Waziz Wildan and Kusmono

Department of Mechanical and Industrial Engineering, Universitas Gadjah Mada, Yogyakarta, Indonesia

Edi Suharyadi

Departement of Physics, Universitas Gadjah Mada, Yogyakarta, Indonesia

\* Corresponding author. E-mail: muhsadathamzah@gmail.com

DOI: 10.14416/j.asep.2025.06.008

Received: 18 March 2025; Revised: 29 April 2025; Accepted: 22 May 2025; Published online: 26 June 2025

© 2025 King Mongkut's University of Technology North Bangkok. All Rights Reserved.

## Abstract

The influence of nano-sized barium titanate addition on the compressive strength and output voltage of silica/barium titanate nanocomposites was investigated. Nano silica powder, synthesized from silica sand via an alkaline fusion method assisted by 200 Hz speaker membrane vibration, was combined with nano barium titanate using the solid-state method at 10, 20, 30, and 40 wt% variations. Samples were uniaxially compacted at 75 MPa and sintered at 1390 °C for 2 hours under atmospheric conditions. The highest bulk density (2.72 g/cm<sup>3</sup>) and compressive strength (37.01 MPa) were achieved at 10 wt% barium titanates. XRD analysis revealed quartz, tridymite, and cristobalite phases and the emergence of fresnoite (Ba<sub>2</sub>TiSi<sub>2</sub>O<sub>8</sub>) and BaTiSiO<sub>5</sub> phases at higher BT contents. The maximum output voltage (5.51 mV) was obtained at 40 wt% barium titanate, indicating the material's potential for piezoelectric applications.

**Keywords:** Barium titanate, Compressive strength, Output voltage, Piezoelectric, Silica

## 1 Introduction

Piezoelectric ceramics are widely used in various high-tech fields, such as sensors, actuators, electronics, and energy harvesters [1]–[3]. The advancement of piezoelectric materials and the structural design of piezoelectric nanogenerators (PENG) tailored for specific applications have been thoroughly explored. Applications of PENG across various sectors, including energy harvesting, sensing systems, biomedical electronics, and emerging innovative sensing technologies, have also been comprehensively reviewed [4]. Ceramic particles effectively obstruct the movement of dislocations, which suppresses plastic deformation and enhances the composite's overall mechanical strength [5]. In the last decade, many countries or regions have reduced

the use of electronic equipment made from lead oxide because of its impact on human and environmental sustainability. Therefore, a new material free of lead that can be used long-term is needed. One natural material that can be used as a substitute for lead is silica (quartz).

Silica, a chemical compound with the molecular formula SiO<sub>2</sub> (silicon dioxide), can be produced from various sources, including mineral sands, plants, and agricultural waste. This material is highly valued due to its abundant availability, eco-friendly nature, ease of synthesis, strong mechanical properties, excellent chemical stability, and ability to withstand high temperatures [6]. Silica also has electrical properties [7]. Silica is a non-metallic material that is non-toxic and pollution-free [8]. Silica is widely used in various applications, including concrete mixes [9], bone tissue



engineering and biosensors [10], biomedical [11], [12], energy diversion materials and lithium battery filling materials [13], [14]. The fabrication of nanocomposite materials for antifungal packaging based on polystyrene has been explored [15]. However, in terms of electricity properties, silica has low dielectric and piezoelectric (output voltage) properties. Therefore, an effort should be made to improve such properties. An alternative to do so is to add barium titanate to silica.

Barium titanate with a tetragonal perovskite crystal structure as a ferroelectric ceramic material is widely used in various applications, such as multi-layer capacitors, detectors, thermistors, and transducers [16]. Barium titanate has a cubic structure at high temperatures. At room temperature, a tetragonal phase, lead-free barium titanate has excellent ferroelectric properties and a high dielectric constant [17].

In the previous study, barium titanate was widely used as a piezoelectric material, such as an energy harvester [18], and sensors [19], and actuators [20]. Hamzah *et al.*, conducted a study to investigate how different sintering temperatures of nano silica affect its physical, mechanical, dielectric, and output voltage characteristics. Their findings revealed that the highest bulk density and relative density,  $2.49 \pm 0.03 \text{ g/cm}^3$  and  $94.03 \pm 0.01\%$ , were achieved when sintered at  $1390 \text{ }^\circ\text{C}$ . X-ray diffraction (XRD) analysis of the sintered silica showed the presence of quartz, tridymite, and cristobalite phases, with the most prominent peak corresponding to cristobalite. The compressive strength and diametral tensile strength were also highest at  $1390 \text{ }^\circ\text{C}$ , measuring  $17.23 \pm 0.27 \text{ MPa}$  and  $6.06 \pm 0.71 \text{ MPa}$ , respectively [7], [21]. Zheng *et al.*, investigated silica-based ceramics reinforced with SiC fibers fabricated using stereolithography. The study focused on examining the effect of SiC fiber content on the mechanical properties of the resulting ceramics. The results demonstrated that as the SiC fiber content increased, the linear shrinkage progressively decreased. Meanwhile, both room-temperature and high-temperature flexural strengths initially improved before declining. When the SiC fiber content reached 4.0 wt%, the linear shrinkage was reduced to 0.62%, primarily due to the oxidation of SiC [22]. Chomyen *et al.*, investigated the influence of fly ash incorporation on the physical, dielectric, and piezoelectric properties of 0–3 barium zirconate titanate–Portland cement composites. The findings revealed that the dielectric

constant decreased with higher fly ash content. In contrast, the piezoelectric coefficient ( $d_{33}$ ) of the composite containing 10% fly ash by volume remained comparable to that of the composite without fly ash [16]. Hu *et al.*, also conducted a study on lead-free piezoelectric ceramics based on barium titanate, synthesized using a simple modified solid-state method employing nano-scale precursors. Piezoelectric characterization revealed that the samples sintered at this temperature exhibited the highest dielectric constant ( $\epsilon_r$ ) of 3533, remnant polarization ( $P_r$ ) of  $16.24 \text{ } \mu\text{C/cm}^2$ , and piezoelectric coefficient ( $d_{33}$ ) of  $420 \text{ pC/N}$ . [23].

Although several studies have previously explored similar materials, research on the mechanical properties and piezoelectric (output voltage) characteristics of silica/barium titanate nanocomposites remains limited. Therefore, this study addresses that gap by developing a new silica-based material. We have also included a discussion of the challenges encountered during the synthesis and characterization processes.

## 2 Experimental Methodology

### 2.1 Materials

Barium titanate powder with a density of  $6.08 \text{ g/cm}^3$  and an average size of 180 nm was purchased from Nanography Turkey. The nano-silica particles used had a purity of 99.31% and an average size of 207.4 nm, which were synthesized from silica sand using the alkaline fusion method assisted by a 200 Hz speaker vibration. Silica sand was obtained from Poso Regency, Central Sulawesi, Indonesia. The sodium hydroxide and hydrochloric acid used in this work were purchased from Merck.

### 2.2 Experimental setup

Silica/barium titanate nanocomposite with barium titanate content of 10%, 20%, 30%, and 40% weight fraction (wt%), each mixture was coded BT10, BT20, BT30, and BT40. The mixture was prepared using a tubular mixer (Stuart Scientific, UK) and mixed for 45 minutes. The green body is formed by applying a uniaxial pressure of 75 MPa in the compaction process. The green body is cylindrical, with a diameter of 15 mm and a thickness of 3.5 mm. The green body was sintered at  $1390 \text{ }^\circ\text{C}$  and held for 2 h in a Carbolite furnace in an air atmospheric environment.

Silica/barium titanate nanocomposite phase structure analysis was performed by X-ray Diffraction (Malvern PANalytical type HR-XRD Empyrean DY 3831, Netherland) using Cu K $\alpha$  radiation (1.5405Å), a diffraction angle range of 2 $\theta$  from 5° to 90°, an increment angle of 0.03°, and a scanning speed of 3°/min. SEM observed the silica/barium titanate morphology. Energy Dispersion Spectrometer (EDS) coupled with SEM was used for chemical analysis. The specimen for SEM observation was thermally etched at a temperature of 1300 °C for 30 min. Archimedes principle in the mercury medium determined the bulk density of sintered composite samples. The Triplicate of each sample was used to measure the average density.

The compressive strength was tested using the Torsen universal testing machine. The method used to measure compressive strength refers to the ASTM C 1424-04 standard. Equation (1) is used to calculate compressive strength as follows:

$$\sigma_c = \frac{F}{A} \quad (1)$$

where  $\sigma_c$  is compressive strength, F is maximum load, and A is cross-sectional area of the test sample. The

output voltage on the silica/barium titanate nanocomposite was measured using Arduino as a microcontroller. Arduino has been utilized to measure the electrical voltage signal magnitude [7]. It is employed to quantify the electrical voltage generated under mechanical stress. As a microcontroller, arduino is used to characterize the output signals of the nanocomposite. Oscilloscopes are known for their ability to measure a wide range of AC and DC voltages, and they are typically used for fault detection in circuits. Additionally, oscilloscopes can measure frequency and signal phase [24]. In this study, arduino was selected as a practical and cost-effective solution to measure output voltage and collect baseline data on the generator system's performance. Although it has limitations in resolution and accuracy compared to standard equipment such as an oscilloscope or source meter, the arduino setup, which includes a load cell, allows for simultaneous measurement of external force and voltage, providing reliable data on output voltage behavior, especially for DC or rectified AC signals. The system was calibrated using a commercial piezoelectric device with a known output voltage magnitude.

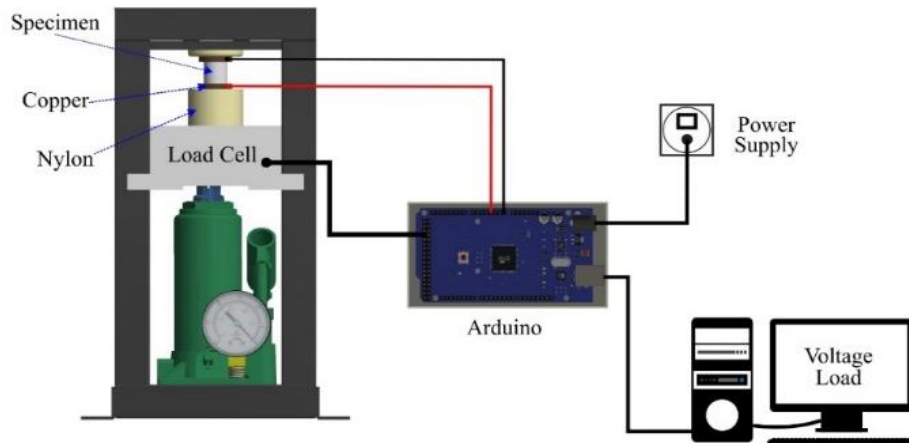


**Figure 1:** Schematic of a piezoelectric testing tool [7].

The schematic of the voltage magnitude test setup is shown in Figure 1. An operational amplifier, or Op-Amp, is a category of linear ICS (integrated circuits) that boost electrical signals. Constructed using a network of transistors, resistors, capacitors, and diodes within a single chip, the Op-Amp is engineered to deliver significant signal amplification across a broad range of frequencies. It operates by

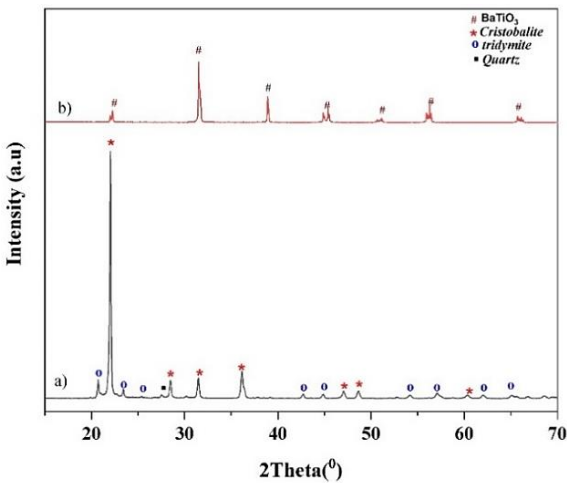
receiving and amplifying an input signal, regardless of its initial magnitude. Depending on the configuration and application, the amplified output typically manifests in terms of voltage, current, or frequency.

The thermal characteristics were analyzed using differential thermal analysis (DTA) of Hitachi STAA7300 Japan, to record the DTA curve. Measurements were made by placing 26 mg of the

sample in a crucible and heating with a temperature interval of 30–1400 °C at a heating rate of 10°C/min under oxygen atmosphere conditions. The differential thermal analysis was analyzed using NETZSCH Proteus Thermal Analysis 8.0.3 software.

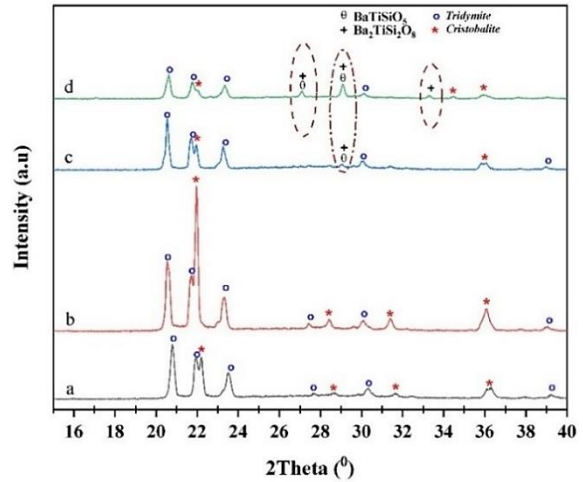
### 3 Results and Discussion

Figure 2(a) shows the XRD patterns of sintered nano silica particles at 1390 °C. The nano-silica particles indicated that the phases formed were tridymite and cristobalite (database\_code\_amcsd 0000531, 0001629). Figure 2(b) shows the XRD pattern of 100% barium titanate, where all the peaks in the pattern belong to barium titanate and are in the cubic phase.



**Figure 2:** XRD pattern of silica and barium titanate with sintering temperature of 1390 °C: (a). Nanosilika; (b). Barium titanate.

Figure 3 shows the diffraction pattern of a silica/barium titanate nanocomposite sintered at 1390 °C, the peaks are visible without noise. In the composition of BT10 and BT20, the phases formed are tridymite and cristobalite, and new phases have started to appear, but the peaks are still weak. At BT30 and BT40, it was confirmed that cristobalite, tridymite, and secondary phases, namely  $\text{BaTiSiO}_5$  and  $\text{Ba}_2\text{TiSi}_2\text{O}_8$  (fresnoite), based on a review of the three prominent peaks.



**Figure 3:** XRD patterns of silica/barium titanate nanocomposite with a sintering temperature of 1390 °C at various compositions: (a). BT10; (b). BT20; (c). BT30; (d). BT40.

The fresnoite phase at an angle of  $2\theta$  shows a diffraction pattern related to the crystal index plane (hkl), which is  $29.09^\circ$  (211);  $27.09^\circ$  (201);  $33.28^\circ$  (310), and  $\text{BaTiSiO}_5$ , which is  $29.06^\circ$  (102);  $27.10^\circ$  (201). The phase corresponds to the AMCS D card number (database\_code\_amcsd 0000531, 0001629) and software high score. This study is in line with previous research, which reported that the addition of barium titanate to silica in large quantities would produce a secondary phase was fresnoite [21], [25].

#### 3.1 Morphology of the silica/barium titanate nanocomposite

SEM observations were carried out to determine the morphology of silica and barium titanate nanoparticles, as shown in Figure 4. The nano-silica particles are irregular, spherical, and agglomerated. In barium titanate particles, the shape is regular and spherical, and agglomeration occurs. After sintering, several specific changes occur in the composite, including the appearance of liquid on the surface. SEM observations confirmed changes in structure, grain size, porosity, and agglomeration of BT0, BT10, BT20, BT30, and BT40, as shown in Figure 5.

The microstructure of nano-silica/barium titanate particle composites sintered at 1390 °C can be seen in Figure 5. Compared to pure silica (BT0), BT10 and BT20, BT10 show more homogeneous grain growth and much less porosity. In the composite with 0% BT, the porosity value is recorded at 6.0 with a relative

percentage of 0.940. As the BT content increases, at 10% BT, the porosity decreases to 3.050, and the relative percentage slightly increases to 0.969. However, as the BT percentage increases further to 20% and 30%, the porosity increases significantly, reaching 9.287 and 14.613, with relative percentages

of 0.907 and 0.854, respectively. BT20 displays an unclear grain surface shape due to melting on the composite surface. At BT30 and BT40, the grain shape is irregular, and the grain boundaries are unclear. The grain shapes are regular at 100% barium titanate, and the grain boundaries are visible.

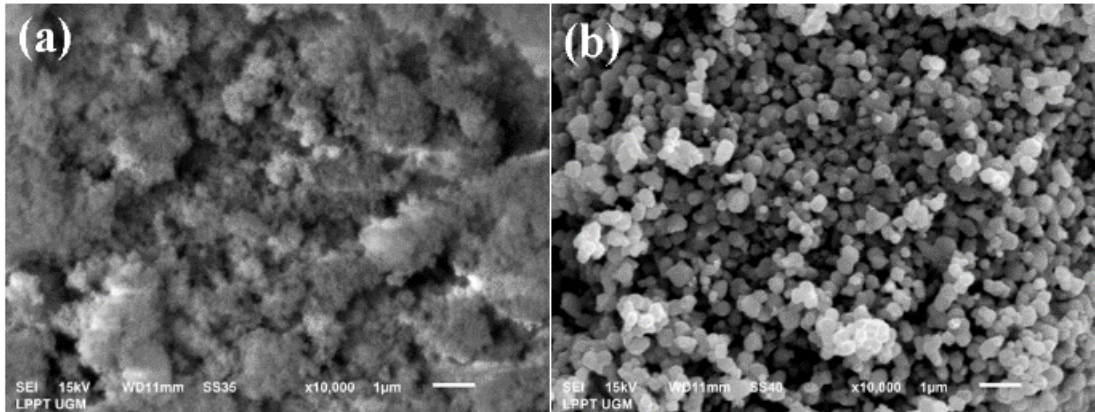


**Figure 4:** Images of powder using SEM: (a). Silica; (b). Barium titanate.

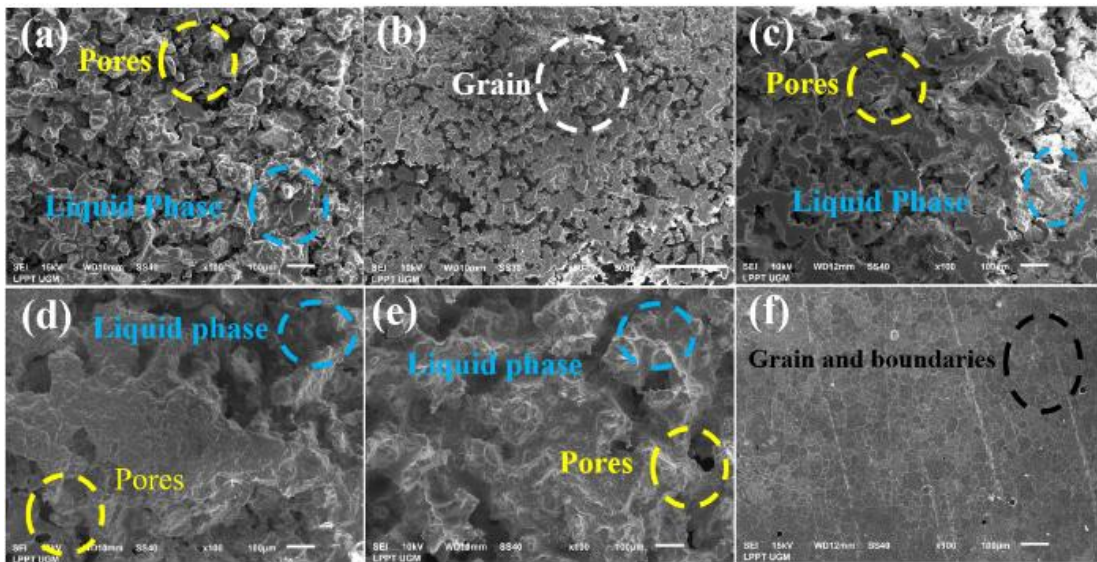


**Figure 5:** SEM image of silica/barium titanate nanocomposite sintered at 1390°C with various barium titanate compositions, a). BT0, b). BT10, c). BT20, d). BT30, e). BT40, f). BT100.

The bonds between the particles are strong due to the sintering temperature. On the other hand, much porosity is formed during sintering. The least porosity is found in the BT10 composite, and it can be concluded that the optimum composition is found in BT10 sintered at 1390 °C. In general, the composite surface shows the presence of a liquid phase, as shown in Figure 5.

The liquid phase produced in nano silica/barium titanate composites sintered at high temperatures will likely come from oxide melts. The liquid phase can improve inter-particle bonding and mechanical properties. This study's results align with silica-based research that sintered at high temperatures produces a liquid phase that improves grain bonding and mechanical properties of ceramics [26].

### 3.2 EDX test results for barium titanate and silica/barium titanate nanocomposite

Tests were carried out using energy-dispersive X-ray analysis for the composition analysis of various variations of barium titanate and silica/barium titanate nanocomposites. The results of the EDX test, as shown in Figures 6 and 7, show that the elements contained in barium titanate, when viewed from the % mole of atoms, are dominated by O (19.73%), Ti (23.07%), and Ba (57, 20%). In contrast, in the silica/barium titanate nanocomposite, when viewed from the % mole of atoms, the elements are dominated by O (62.00%), Si (30.98%), Ti (2.40%), and Ba (4.62%). Ba and Ti elements are the leading indicators of the piezoelectric phase of  $\text{BaTiO}_3$ , which has a perovskite structure with high piezoelectric properties.

The oxygen element forms a stable oxide network in the perovskite structure, and its deficiency can cause lattice defects that negatively affect the material's polarity. Meanwhile, the Si element comes from the silica matrix and has no direct contribution to the piezoelectric properties, but can form secondary phases such as  $\text{Ba}_2\text{TiSi}_2\text{O}_8$  or  $\text{BaTiSiO}_5$ , which have the potential to disrupt the continuity of the perovskite phase and reduce piezoelectric performance. Increasing the proportion of Ba and Ti is generally positively correlated with the increase in piezoelectric response, if the perovskite structure is maintained. Conversely, an excessive increase in Si content can cause the formation of non-piezoelectric phases, reduce homogeneity, and disrupt domain orientation, thereby reducing piezoelectric output. Therefore, the composition ratio between elements is critical to control and optimize the piezoelectric performance of the resulting nanocomposite.

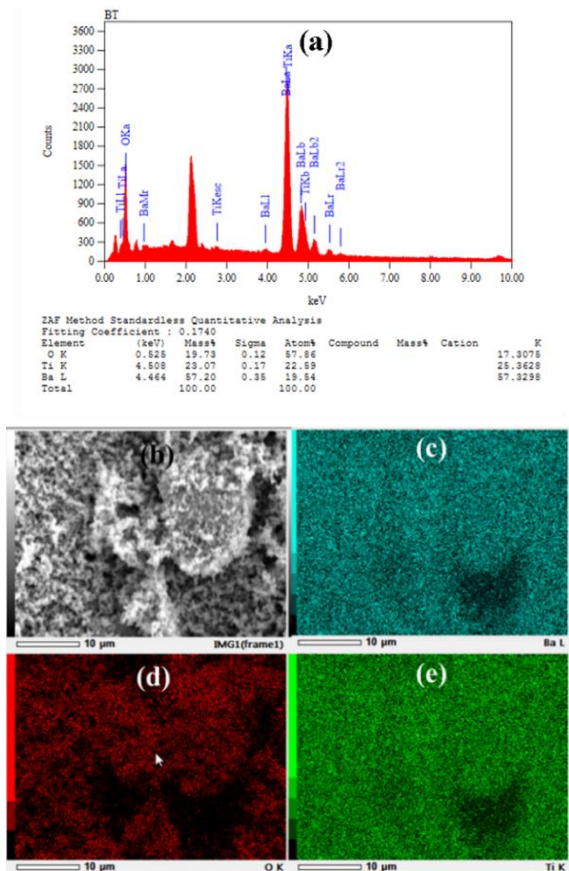


**Figure 6:** SEM/EDX test results for barium titanate powder: (a). The results of the distribution of EDS elements; (b). SEM photos; (c). Element of Ba; (d). Elements of O; (e). Ti element.

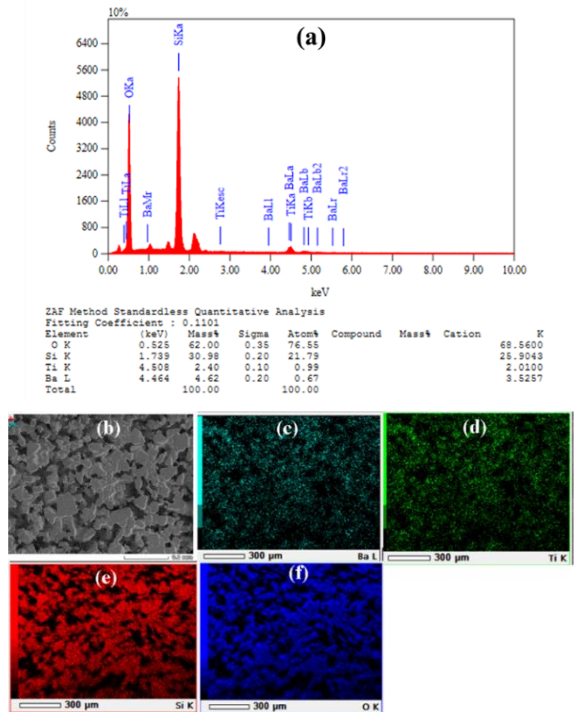


**Figure 7:** SEM/EDX test results for silica/barium titanate nanocomposite (BT10): (a). The results of the distribution of EDS elements; (b). SEM photos; (c). Element of Ba; (d). Element of Si; (e). Element of Ti; (f). Element of O.

### 3.3 Bulk density

Figure 8 shows the result of bulk density measurement using Archimedes' principle. The results showed a change in bulk density with an increasing weight% of barium titanate. In the composition of BT10, BT20, and BT30, the bulk density experienced an insignificant increase. At BT40, the bulk density of the specimen decreased significantly. The highest bulk density occurs at BT10 due to the sintering temperature of 1390 °C, which is suitable so that densification occurs between the particle surfaces.

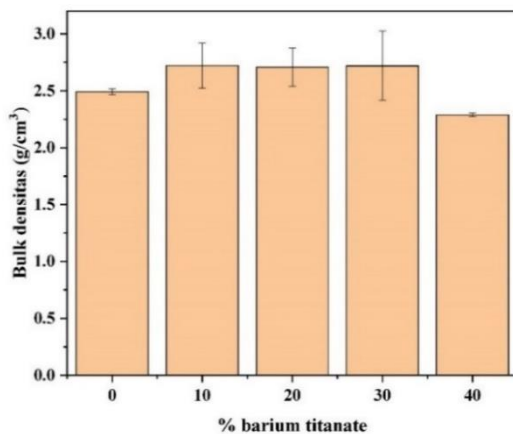


**Figure 8:** Effect of weight % of barium titanate on the bulk density of silica/barium titanate nanocomposites.

The decreased bulk density of the specimen at the BT40 was due to the increased porosity. This can be seen in the SEM photo in Figure 5. The increase in porosity is probably due to the very high sintering temperature of silica/barium titanate nanocomposite with increasing barium titanate variations or a decrease in sintering temperature with increasing barium titanate. The sintering temperature suitable for densification between barium titanate particles is 1350 °C [27], so the more barium titanate content, the porosity of the silica/barium titanate nanocomposite will increase, as shown in Figure 5.

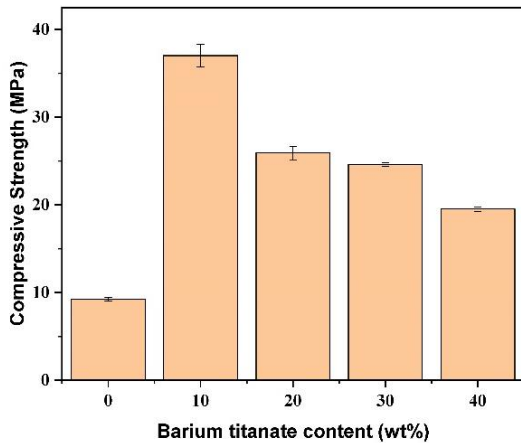
Given the relatively stable bulk density values observed between BT10 and BT30 compositions, there is an opportunity to optimize the material formulation by reducing the amount of barium titanate without significantly affecting the targeted density-related properties. Lowering the barium titanate content while preserving comparable material performance presents notable advantages, particularly

cost savings and improved manufacturing efficiency. As a result, identifying an optimal filler concentration within this range not only maintains the mechanical integrity of the composites but also enhances the economic feasibility of silica/barium titanate nanocomposite production.

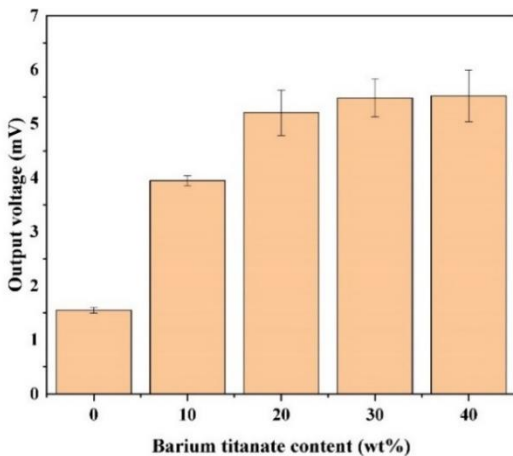
### 3.4 Compressive strength

Figure 9 shows the results of compressive strength testing of nano silica and BT10, BT20, BT30, and BT40 sintered at 1390 °C. The test results show increased compressive strength properties with each addition of barium titanate. Compressive strength values respectively 9.24, 37.01, 25.91, 24.59, and 19.51 MPa. The highest compressive strength value occurs at BT10 of 37.01 MPa; the increase in compressive strength is due to the high density at BT10. The compressive strength of the composites is observed to peak at 10 wt% barium titanates (BT10), followed by a gradual decline with further increases in BT content. This behavior is primarily attributed to the rise in porosity and elasticity caused by the excessive addition of barium titanate, which compromises the structural cohesion and diminishes the material's capacity to endure compressive loads beyond the optimal composition. To provide a clearer understanding, a combined graph comparing bulk density and compressive strength has been proposed, emphasizing the correlation between material density and mechanical performance. From a practical perspective, the BT10 composition achieves the most favorable balance between bulk density and compressive strength, positioning it as the optimal choice for applications that demand superior structural integrity. On the other hand, although higher barium titanate contents may offer advantages in terms of piezoelectric enhancements, they lead to a reduction in compressive strength, thus requiring careful consideration when selecting materials based on specific application needs.

The composite density caused by the sintering of atoms in the particles diffuses across the particle boundaries, fusing the particles, thus forming a nearly perfect solid part. However, the compressive strength decreased as the barium titanate composition increased. The decrease in compressive strength is affected by the amount of porosity, which increases with the increase in barium titanate composition. The increased porosity was due to the high sintering temperature of barium titanate.



**Figure 9:** Effect of weight % of barium titanate on the compressive strength of silica/barium titanate nanocomposites.



**Figure 10:** Effect of weight % of barium titanate on the output voltage of silica/barium titanate nanocomposites.

### 3.5 The output voltage of the silica/barium titanate nanocomposite

The silica/barium titanate nanocomposites output voltage has piezoelectric properties. Suppose no mechanical stress is applied to the silica/barium titanate nanocomposite material. In that case, the output voltage is zero because the electric dipole is still in equilibrium, so no electric polarization occurs. On the other hand, if the composite is subjected to mechanical stress, it will cause external stress, as shown in Figure 10.

Figure 10 shows the output voltage results on nano-silica particles and nanocomposites BT10,

BT20, BT30, and BT40 sintered at 1390 °C. The test results show an increase in the output voltage value for each addition of barium titanate. The output voltage values are 1.58, 3.95, 5.21, 5.48, and 5.51 mV, respectively. This trend highlights the important role of barium titanate in enhancing piezoelectric performance, which is attributed to its inherent material properties. However, when these results are compared with findings from bulk density and compressive strength measurements, it becomes clear that higher barium titanate content increases electrical output, resulting in greater porosity and compromising mechanical strength. This highlights the critical balance that must be maintained between mechanical integrity and piezoelectric efficiency. Furthermore, compared to polymer-based piezoelectric composites [28], which generally offer superior flexibility but lower output voltage, silica/barium titanate nanocomposites present an attractive alternative for industrial applications requiring high electrical performance and adequate structural stability.

The output voltage increased from 1.58 mV to 5.51 mV. The highest output voltage value occurs in BT40 of 5.51 mV MPa. The increase in the output voltage occurs at BT40 because the high content of BT is dispersed on the surface of the silica/barium titanate ceramic nanoparticles, causing continuous polarization. In BT30 and BT40, secondary phases are formed, namely  $\text{BaTiSiO}_5$  and  $\text{Ba}_2\text{TiSi}_2\text{O}_8$ , where these phases generally include single crystals with good piezoelectric, dielectric, and optical properties. The thermal and electrical properties of  $\text{Ba}_2\text{TiSi}_2\text{O}_8$  crystals indicate their potential as alternative materials for high-temperature piezoelectric sensors [29]. The magnitude of the output stress is affected by defects in the material; the more significant the defect, the smaller the output value [30]. BT40 shows the smallest bulk density, as shown in Figure 7, so it can be concluded that the high weight fraction of barium titanate contributes to the increased output stress in the nano-silica/barium titanate particle composite. Barium titanate is a material that has high piezoelectric properties, so with an increase in the weight fraction of barium titanate, its piezoelectric properties will increase [25], [31]. Figure 3 shows that a new phase appears in  $\text{BaTiSi}_2\text{O}_5$  and  $\text{Ba}_2\text{TiSi}_2\text{O}_8$  (BTS), in which this phase is tetragonal, which is a strong source of spontaneous polarization in crystals. The crystal polarization of BTS shows excellent quality, affecting the output voltage value (piezoelectricity).

BTS crystals show good dielectric, optical, and piezoelectric properties.

Figure 11 illustrates the relationship between dielectric constant and dielectric loss as frequency functions at room temperature, within the 10 to 500 kHz range. The graph reveals that the dielectric constant and dielectric losses exhibit higher values at lower frequencies, followed by a decline as frequency increases, eventually stabilizing at higher frequencies. This behavior is a typical characteristic of dielectric materials.

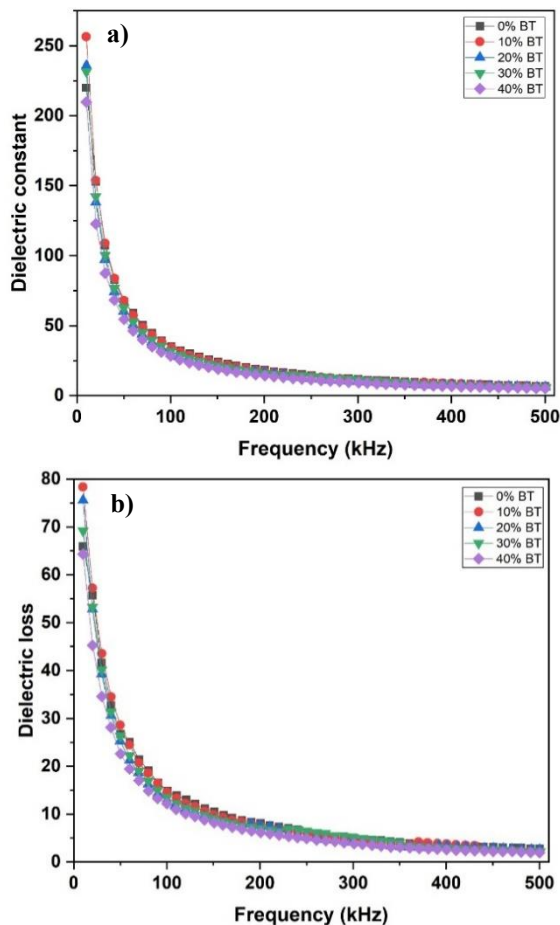


**Figure 11:** Frequency-dependent plot of permittivity for BT0, BT10, BT300, and BT40, (a) dielectric constant, and (b) dielectric loss.

As shown in Figure 11(a), the constant dielectric values for BT 0, BT 10, BT 20, BT 30, and BT 40% samples are initially high at low frequencies and decline sharply with increasing frequency, reaching a

steady state beyond 250 kHz. Such a trend is common among dielectric materials: at low frequencies, various polarization mechanisms, including dipolar, interfacial, ionic, and electronic polarization, can effectively respond to the external electric field. However, at higher frequencies, only electronic polarization can follow the rapid oscillations of the field, resulting in a notable decrease in dielectric constant values. Although adding barium titanate generally enhances the dielectric constant due to its intrinsically high dielectric properties, the results of this study indicate that increasing the barium titanate volume fraction from 10% to 40% does not significantly improve the dielectric constant. This phenomenon is attributed to the rise in porosity accompanying higher barium titanate content. The increase of porosity stems from differences in sintering behavior and particle size mismatch between barium titanate and silica, forming voids during consolidation. Higher porosity adversely affects the material's charge storage capacity, as the air within the pores has a substantially lower dielectric constant.

Meanwhile, Figure 11(b) shows a similar trend in dielectric loss: high values at lower frequencies, with a sharp decrease at higher frequencies. Elevated dielectric losses at low frequencies are mainly caused by charge accumulation at grain boundaries through interfacial polarization, where restricted charge mobility occurs. As the frequency increases, the interface cannot respond quickly enough, resulting in lower dielectric losses. Increasing barium titanate content notably correlates with reduced dielectric loss at high frequencies, suggesting that greater porosity limits charge migration pathways and reduces energy dissipation. In summary, although barium titanate enhances dielectric properties, its addition in silica-based systems must be carefully optimized, as excessive porosity can undermine the overall dielectric performance.

The DTA curve in Figure 12 shows that an exothermic peak occurs during the heating process. At 122.8, 154.7, and 160.0 °C, a peak is formed, probably due to loss of moisture or air molecules bound to the pores of the silica or barium powder. At a temperature of 550 °C to 800 °C, a peak occurs. At temperatures of 800 °C to 1400 °C, weak peaks also appear. The peak in Figure 13 is associated with the phase changes that occur in silica. Based on the thermal behavior of silica at temperatures of 570–870 °C, quartz is formed, and tridymite is formed at temperatures of 870–1470 °C [32].

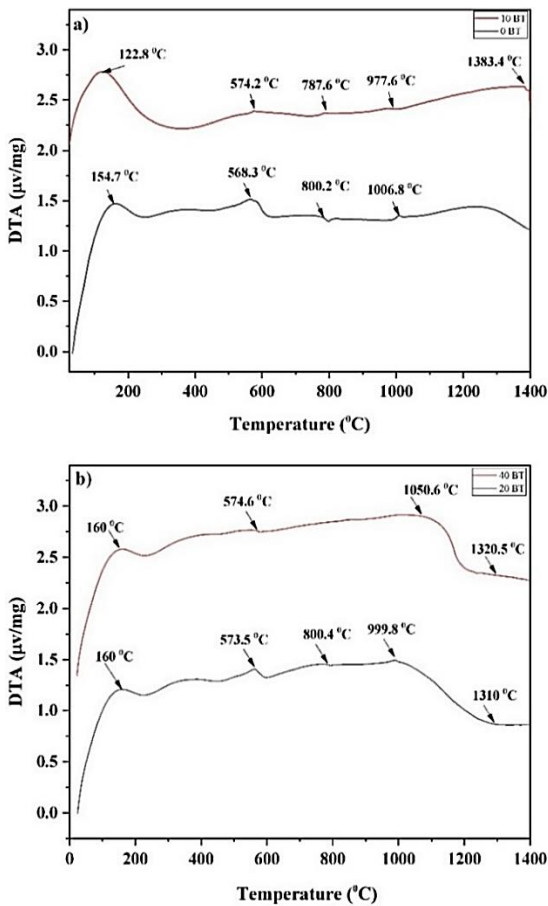


**Figure 12:** Differential thermal analysis curves at (a) BT0 and BT10, (b) BT20 and BT40.

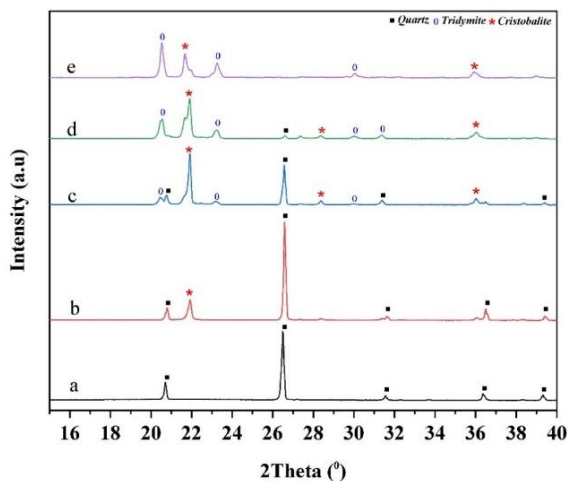


**Figure 13:** XRD pattern of silica powder at: (a) 510 °C; (b) 700 °C; (c) 910 °C; (d) 1100 °C; (e) 1400 °C.

The XRD test results prove the phase transformation that occurs in silica at each temperature, as shown in Figure 13. In Figure 13, the quartz phase transforms into the cristobalite phase at temperatures of 700–1400 °C, or the process of forming the cristobalite phase is faster because silica still contains impurities, which can increase the transformation of the quartz phase into the cristobalite phase.

## 4 Conclusions

This research confirms that adding barium titanate influences the physical, mechanical, and piezoelectric properties of silica/barium titanate nanocomposites. The results show that optimizing the barium titanate content, particularly at 10 wt%, leads to superior mechanical performance, as evidenced by the highest recorded bulk density (2.72 g/cm<sup>3</sup>) and compressive strength (37.01 MPa). Furthermore, phase transformations into tridymite, cristobalite, fresnoite, and BaTiSiO<sub>5</sub> were observed at higher barium titanate contents (BT30 and BT40), suggesting the potential to tailor functional characteristics, even though the phase intensities remain relatively low. The highest output voltage, measured at 5.51 mV for BT40, further demonstrates the promising application of these composites in piezoelectric devices.

The main aim of this study was to develop a silica-based composite material with improved mechanical strength and piezoelectric performance through the controlled incorporation of barium titanate. The findings indicate that the resulting nanocomposites offer strong potential for cost-effective, scalable use in energy harvesting, sensor technologies, and innovative material applications, contributing valuable insights for future material development strategies.

## Acknowledgments

The Authors wish acknowledge the Department of Mechanical and Industrial Engineering, Universitas Gadjah Mada, Yogyakarta, Indonesia and the Department of Mechanical Engineering, Universitas Tadulako, Palu, Indonesia.

## Author Contributions

M. S. H.: conceptualization, investigation, reviewing and editing; M. S. H: investigation, methodology,

writing an original draft; M. W. W: research design, data analysis; K.: conceptualization, data curation, writing—reviewing and editing, funding acquisition, project administration; E. S: writing—reviewing, M. S. F: editing and research design. All authors have read and agreed to the published version of the manuscript.

### Conflicts of Interest

The authors declare no conflict of interest.

### References

- [1] D.-J. Shin, S.-J. Jeong, C.-E. Seo, K.-H. Cho, and J.-H. Koh, “Multi-layered piezoelectric energy harvesters based on PZT ceramic actuators,” *Ceramics International*, vol. 41, no. 1, pp. 686–690, 2015, doi: 10.1016/j.ceramint.2015.03.180.
- [2] C. Zhao, Q. Zhang, W. Zhang, X. Du, Y. Zhang, S. Gong, K. Ren, Q. Sun, and Z. L. Wang, “Hybrid piezo/triboelectric nanogenerator for highly efficient and stable rotation energy harvesting,” *Nano Energy*, vol. 57, no. 3, pp. 440–449, 2019, doi: 10.1016/j.nanoen.2018.12.062.
- [3] G. Tian, W. Deng, Y. Gao, D. Xiong, C. Yan, X. He, T. Yang, L. Jin, X. Chu, and H. Zhang, “Rich lamellar crystal baklava-structured PZT/PVDF piezoelectric sensor toward individual table tennis training,” *Nano Energy*, vol. 59, no. 5, pp. 574–581, 2019, doi: 10.1016/j.nanoen.2019.03.013.
- [4] S. Sriphan, T. Charoonsuk, T. Maluangnont, and N. Vittayakorn, “Piezoelectric energy harvesting for low-power smart electronics,” *Encyclopedia of Materials: Electronics*, vol. 1, no. 1, pp. 369–404, 2023, doi: 10.1016/B978-0-12-819728-8.00050-4.
- [5] S. B. Nagaraju, M. Puttegowda, M. K. Somashekara, T. G. T. Girijappa, P. D. Govindaswamy, and K. Sathyanarayana, “Advancing the performance of ceramic-reinforced Aluminum hybrid composites: A comprehensive review and future perspectives,” *Applied Science and Engineering Progress*, vol. 17, no. 2, 2024, Art. no. 7034, doi: 10.14416/j.asep.2023.10.001.
- [6] I. V. Schweigert, K. E. J. Lehtinen, M. J. Carrier, and M. R. Zachariah, “Structure and properties of silica nanoclusters at high temperatures,” *Physical Review B*, vol. 65, no. 23, 2002, Art. no. 235410, doi: 10.1103/PhysRevB.65.235410.
- [7] M. S. Hamzah, M. W. Wildan, Kusmono, and E. Suharyadi, “Effect of sintering temperature on physical, mechanical, and electrical properties of nano silica particles synthesized from Indonesia local sand for piezoelectric application,” *Journal of Asian Ceramic Societies*, vol. 11, no. 1, pp. 178–187, 2023, doi: 10.1080/21870764.2023.2173851.
- [8] M. Ma, H. Li, Y. Xiong, and F. Dong, “Rational design, synthesis, and application of silica/graphene-based nanocomposite: A review,” *Materials & Design*, vol. 198, no. 1, 2021, Art. no. 109367, doi: 10.1016/j.matdes.2020.109367.
- [9] S. Ahmad, O. S. B. Al-Amoudi, S. M. S. Khan, and M. Maslehuddin, “Effect of silica fume inclusion on the strength, shrinkage and durability characteristics of natural pozzolan-based cement concrete,” *Case Studies in Construction Materials*, vol. 17, no. 2, p. 1255, 2022, doi: 10.1016/j.cscm.2022.e01255.
- [10] M. K. Yadav, V. Pandey, K. Mohanta, and V. K. Singh, “A low-cost approach to develop silica doped Tricalcium Phosphate (TCP) scaffold by valorizing animal bone waste and rice husk for tissue engineering applications,” *Ceramics International*, vol. 48, no. 7, pp. 25335–25345, 2022, doi: 10.1016/j.ceramint.2022.05.207.
- [11] Q. Lei, J. Guo, A. Noureddine, A. Wang, S. Wuttke, C. J. Brinker, and W. Zhu, “Sol–gel-based advanced porous silica materials for biomedical applications,” *Advanced Functional Materials*, vol. 30, no. 41, 2020, Art. no. 1909539, doi: 10.1002/adfm.201909539.
- [12] G. J. Owens, R. K. Singh, F. Foroutan, M. Alqaysi, C.-M. Han, C. Mahapatra, H.-W. Kim, and J. C. Knowles, “Sol–gel based materials for biomedical applications,” *Progress in Materials Science*, vol. 77, no. 4, pp. 1–79, 2016, doi: 10.1016/j.pmatsci.2015.12.001.
- [13] M.-R. Buga, A. A. Spinu-Zaulet, C. G. Ungureanu, R.-A. Mitran, E. Vasile, M. Florea, and F. Neatu, “Carbon-coated SiO<sub>2</sub> composites as promising anode material for Li-ion batteries,” *Molecules*, vol. 26, no. 15, p. 4531, 2021, doi: 10.3390/molecules26154531.
- [14] B. Huang, B. Chu, T. Huang, and A. Yu, “Nitrogen-doped carbon-coating disproportionated SiO materials as long cycling stable anode for lithium ion batteries,”

- Molecules*, vol. 26, no. 6, p. 1536, 2021, doi: 10.3390/molecules26061536.
- [15] T. Thirugnanasambandan, S. M. K. Thiagamani, S. Siengchin, and S. M. Rangappa, "Fabrication and characterization of an active nanocomposite film based on polystyrene/thyme/nano ZnO for food packaging," *Applied Science and Engineering Progress*, vol. 16, no. 3, 2023, Art. no. 6440, doi: 10.14416/j.asep.2022.11.003.
- [16] J. S. Park and Y. H. Han, "Nano size BaTiO<sub>3</sub> powder coated with silica," *Ceramics International*, vol. 31, no. 6, pp. 777–782, 2005, doi: 10.1016/j.ceramint.2004.09.003.
- [17] Z.-J. Shen, S. Esnault, A. Schinzel, C. Borner, and J. S. Malter, "The peptidyl-prolyl isomerase Pin1 facilitates cytokine-induced survival of eosinophils by suppressing Bax activation," *Nature Immunology*, vol. 10, no. 3, pp. 257–265, 2009, doi: 10.1038/ni.1697.
- [18] D. Hu, M. Yao, Y. Fan, C. Ma, M. Fan, and M. Liu, "Strategies to achieve high performance piezoelectric nanogenerators," *Nano Energy*, vol. 55, no. 1, pp. 288–304, 2019, doi: 10.1016/j.nanoen.2018.10.053.
- [19] P. Chomyen, R. Potong, R. Rianyo, A. Ngamjarrojana, P. Chindaprasirt, and A. Chaipanich, "Microstructure, dielectric and piezoelectric properties of 0–3 lead free barium zirconate titanate ceramic-Portland fly ash cement composites," *Ceramics International*, vol. 44, no. 1, pp. 76–82, 2018, doi: 10.1016/j.ceramint.2017.09.112.
- [20] Y. Wu, J. Zhang, Y. Tan, and P. Zheng, "Notable grain-size dependence of converse piezoelectric effect in BaTiO<sub>3</sub> ceramics," *Ceramics International*, vol. 42, no. 8, pp. 9815–9820, 2016, doi: 10.1016/j.ceramint.2016.03.075.
- [21] D. E. Rase and R. Roy, "Phase equilibria in the system BaTiO<sub>3</sub>-SiO<sub>2</sub>," *Journal of the American Ceramic Society*, vol. 38, no. 11, pp. 389–395, 1955, doi: 10.1111/j.1151-2916.1955.tb14562.x.
- [22] Y. Lee, C. Lin, W. Lu, W. Chen, and W. Lee, "Influence of SiO<sub>2</sub> addition on the dielectric properties and microstructure of (Ba<sub>0.96</sub>Ca<sub>0.04</sub>)(Ti<sub>0.85</sub>Zr<sub>0.15</sub>) O<sub>3</sub> ceramics," *International Journal of Applied Ceramic Technology*, vol. 6, no. 6, pp. 692–701, 2009, doi: 10.1111/j.1744-7402.2009.02379.x.
- [23] M. S. Hamzah, M. W. Wildan, Kusmono, and E. Suharyadi, "Study of the synthesis of nanosilica particles from silica sand Poso Regency for the development of piezoelectric materials," Ph.D. dissertation, Department of Mechanical and Industrial Engineering, Universitas Gadjah Mada, Indonesia, 2023.
- [24] A. S. Morris and R. Langari, *Measurement and Instrumentation Theory and Application*. New York: Academic Press, pp. 1–703, 2016. doi:10.1016/C2013-0-15387-1
- [25] Y. Slimani, A. Selmi, E. Hannachi, M. A. Almessiere, G. AlFalah, L. F. AlOusi, G. Yasin, and M. Iqbal, "Study on the addition of SiO<sub>2</sub> nanowires to BaTiO<sub>3</sub>: Structure, morphology, electrical and dielectric properties," *Journal of Physics and Chemistry of Solids*, vol. 156, no. 9, 2021, Art. no. 110183, doi: 10.1016/j.jpics.2021.110183.
- [26] W. Zheng, J. M. Wu, S. Chen, K. B. Yu, J. Zhang, and Y. S. Shi, "Improved mechanical properties of SiC fiber reinforced silica-based ceramic cores fabricated by stereolithography," *Journal of Materials Science & Technology*, vol. 116, no. 7, pp. 161–168, 2022, doi: 10.1016/j.jmst.2021.12.012.
- [27] S. Hu, C. Luo, P. Li, J. Hu, G. Li, H. Jiang, and W. Zhang, "Effect of sintered temperature on structural and piezoelectric properties of barium titanate ceramic prepared by nano-scale precursors," *Journal of Materials Science: Materials in Electronics*, vol. 28, no. 7, pp. 9322–9327, 2017, doi: 10.1007/s10854-017-6670-7.
- [28] F. Mokhtari, B. Azimi, M. Salehi, S. Hashemikia, and S. Danti, "Recent advances of polymer-based piezoelectric composites for biomedical applications," *Journal of the Mechanical Behavior of Biomedical Materials*, vol. 122, no. 10, 2021, Art. no. 104669, doi: 10.1016/j.jmbbm.2021.104669.
- [29] S. Cao, B. Jiang, Y. Zheng, X. Tu, K. Xiong, P. Gao, and E. Shi, "The growth and thermal, electrical properties characterization of Ba<sub>2</sub>TiSi<sub>2</sub>O<sub>8</sub> piezoelectric crystal," *Journal of Crystal Growth*, vol. 451, no. 10, pp. 207–213, 2016. doi: 10.1016/j.jcrysgro.2016.07.014.
- [30] F. Qi, N. Chen, and Q. Wang, "Preparation of PA11/BaTiO<sub>3</sub> nanocomposite powders with improved processability, dielectric and piezoelectric properties for use in selective laser sintering," *Materials & Design*, vol. 131, no. 10, pp. 135–143, 2017, doi: 10.1016/j.matdes.2017.06.012.



- 
- [31] A. A. Moosa and B. F. Saddam, "Synthesis and characterization of nanosilica from rice husk with applications to polymer composites," *American Journal of Materials Science*, vol. 7, no. 6, pp. 223–231, 2017, doi: 10.1016/j.cscee.2025.101145.
- [32] K. F. Jusnes, M. Tangstad, and E. Ringdalen, "Phase transformations from quartz to cristobalite," in *Extraction 2018: Proceedings of the First Global Conference on Extractive Metallurgy*, pp. 717–727, 2018. doi: 10.1007/978-3-319-95022-8\_56.